Desalination and Water Treatment
www.deswater.com

doi: 10.5004/dwt.2018.23118

136 (2018) 413–421
December

Comparative study of plasma-synthesized and commercial-P25 TiO_2 for photocatalytic discoloration of Reactive Red 120 dye in aqueous solution

Albert P. Mbouopda[a], Elie Acayanka[a,*], Serge Nzali[c], Georges Y. Kamgang[a], Estella B. Njoyim Tamungang[b], Samuel Laminsi[a], Dominique Richard[d,*]

[a]*Inorganic Chemistry Department, University of Yaoundé I, P.O. Box 812, Yaoundé, Cameroon, email: acayanka@gmail.com (E. Acayanka)*
[b]*Laboratory of Noxious Chemistry and Environmental Engineering (LANOCHEE), Department of Chemistry, Faculty of Science, University of Dschang, Dschang, Cameroon*
[c]*School of Wood, Water and Natural Resources, Faculty of Agronomy and Agricultural Sciences, University of Dschang (Ebolowa campus), P.O. Box 786, Ebolowa, Cameroon*
[d]*Laboratoire de Génie des Procédés Catalytiques (UMR5285 CNRS et CPE Lyon), 3, rue Victor Grignard, P.O. Box 82077, 69616 Villeurbanne cedex, France, email: dri@lgpc.cpe.fr*

Received 31 May 2018; Accepted 11 September 2018

ABSTRACT

The photoactivity of titania obtained by exposing 50 mg L^{-1} of $TiCl_3$ precursor to non-thermal plasma was evaluated through the degradation of the reagent RR120 dye. Herein, the effect of calcination has been closely investigated to bring insight into the effect of crystallinity on degradation. As photocatalysis occurs at the surface, BET analysis was run to evaluate the specific surface and pore size diameter. XRD was conducted to follow the crystal phase. Results reveal that the increase in calcination temperature led to an increase in the crystallite size and pore size. The trend towards rutilation observed with increasing temperature makes the material less effective beyond 500°C. The degradation efficiencies when comparing the titania synthesized under plasma condition with the commercial (Evonik P25) are 35% and 98%, respectively. These findings show the great potential of synthesized titania due to its greater contact surface and its particular shape.

Keywords: Non-thermal plasma; Photocatalysis; Titania; Crystallinity; Nanomaterials

1. Introduction

The legislation on toxic substances in industrial wastewater is growing ever stricter; this has led many researchers to examine various purification methods in order to tackle the issue at source. One of the biggest polluters is the chemical industry, mainly the organic coloring industry (34%) [1–3]. Dyes pose enormous pollution problems due to their acute and chronic effects; most of these dyes are carcinogenic and mutagenic [4,5]. Aside from the aesthetic aspect, the other environmental concerns are their ability to absorb and reflect sunlight, which negatively interferes with the growth of bacteria that can degrade impurities in the water.

To remedy, the development of more effective, faster, less expensive and more suitable degradation technique for refractory or toxic organic compounds has been addressed. Many methods of water treatment exist, some as biological and physicochemical treatments, require a lot of space and are expensive. This has led many scientists to propose alternative techniques such as transferring the pollutant from the aqueous phase to solid phase, for example, adsorption, coagulation and precipitation, which have been longer satisfactory [6–8]. But these techniques became ineffective in recent years, due to the exponential increase in the amount and the complexity of discharged pollutants; the formed sludge treatment became a more complex challenge [9,10]. Recently, advanced

* Corresponding authors.

oxidation processes (AOPs) have been widely investigated [11–15]. AOPs mainly involve the generation of a very powerful and non-selective oxidizing agent, the hydroxyl radical $OH^{\bullet}$, generally produced by different methods such as chemical oxidation processes, which use hydrogen peroxide, ozone, irradiation with UV light, or the simultaneous use of these highly exploited reagents and their coupling with catalysts. Much progress have been done since, some results have been achieved thus allowing making choices of the most appropriate for the specific treatment problems. The photocatalysis techniques, for instance, were found especially suitable for degrading azo and anthraquinonic dyes, which are the mostly used textile colorants. Titania is one of the common semiconductors widely used for its photocatalytic activity in water treatment; dye-sensitized solar cells; air purification; self-cleaning coatings; self-sterilizing coatings, etc. [16–20]. Crystallinity, pore volume, phase composition and specific surface area (depending on particle size and shape) of TiO_2 are the key factors to affect its photocatalytic activity, which is relevant to its synthesis technique [21–23]. A fundamental understanding of the characteristics affecting photocatalytic activity is necessary to make efficient use of existing catalysts and to provide design criteria for the preparation of new ones.

Recently we presented a new method to synthesize titania nanorods using the gliding arc process which relates to elevated oxidation observations of reactive species [24]. The use of non-thermal plasma approach has shown some advantages since it is obtained by oxi-precipitation of [Ti^{3+}, $3Cl^{-}$] without any other reagents added. The advantage of using TiO_2 as a photocatalyst combined with non-thermal plasma irradiation lies in additional hydroxyl radicals formed in gaseous discharges and in UV light emitted by the discharge which improves the formation of excited particles and promotes the dissociation of adsorbed water molecules.

The gliding arc plasma device presents a new and inexpensive way of cold plasma generation and was first introduced by Czernichowski's team for the treatment of various gases [25,26]. The device was adapted to a liquid treatment solution like wastewater [27–30]. Nevertheless, the main researches conducted in this domain led to the same drawback: the high energy consumption which increases the cost of treatment. To face this issue, the addition of a catalyst, biosorbent or the study of post-discharge phenomena were conducted and have opened new perspectives for the degradation of recalcitrant pollutants such as persistent organics released into wastewater from textile industries [31–34]. The colored dyes, commonly azoïc and anthraquinonic are often toxic and resistant to conventional treatment techniques and constitute serious threats to public health [33,35]. Their degradation from effluents is, therefore, necessary and has received increasing attention during the past decade.

In the present study, we have used gliding arc plasma process in combination of plasma-synthesized titanium dioxide (TiO_2) as photo-catalysts to achieve an abatement of polluted synthetic wastewater containing the azoic Reactive Red 120 (RR120) dye. Commercial Evonik P25 TiO_2 was also used as a basis for comparison with TiO_2 photocatalyst prepared by plasma approach. Hence, a study of structural characteristics relevant to the photoreactivity and the effect of calcination are developed for a good understanding of the effect of these characteristics.

2. Materials and methods

2.1. Catalysts preparation

The precursor solution ($TiCl_3$) was directly exposed to the plasma gas obtained at atmospheric pressure as presented by Acayanka et al. [24]. The interaction between the non-thermal plasma and the aqueous medium leads to the formation of active species that induce acidifying and oxidizing effects in the target solution. These species are considered to be $NO^{\bullet}$ and $HO^{\bullet}$ radicals formed as a result of electron (or/and photon) impact dissociation of water and nitrogen molecules present in the feeding gas [27,36–38].

2.2. Catalyst characterization methods

Room temperature powder X-ray diffraction patterns were obtained with a D8 Advanced A25 diffractometer (Bruker, France) with a Bragg–Brentano configuration and a linear detector. The X-ray source was a copper long fine focused X-ray diffraction tube operating at 40 kV and 30 mA, with an angular step of 0.015° and a time per step of 0.1 s. Crystalline phases were identified by referencing the PDF 2014 database. The porous structure of the catalyst was assessed from the –196°C N_2 adsorption–desorption isotherms, obtained in a ASAP 2020 (Micromeritics, France). The samples were previously outgassed at 160°C and 5×10^{-3} Torr for 16 h. The specific surface area was calculated from the BET method (S_{BET}). The scanning electron micrographs of the materials were taken with a Philips XL 30 FEG apparatus equipped with a field emission gun operated at 5 kV. The transmission electron microscopy was performed on a Tecnai F30 microscope (field emission cathode, operated at 300 kV) on a material dispersed in butanol and deposited onto a perforated carbon foil supported on a copper grid. Diffused reflectance spectra were obtained from dry-pressed disc samples using a UV–Vis spectrophotometer (UV2550, Shimadzu). $BaSO_4$ was used as the reflectance standard.

2.3. Photocatalytic discoloration experiments

The experimental setup is shown in Fig. 1 [26]. The device consists of a generator (9 kV, 160 mA). The arc formed is blown down along the two electrodes by a gas flow provided by a compressor and directed along the axis of the electrodes where it bursts into a plasma plume until it is replaced by a new arc. During this movement, the temperature of the plasma falls and it becomes closer to the ambient temperature at atmospheric pressure. The plasma plume is directed to be in contact with the target–plasma interface so that the reactive species formed in the discharge can react at the gas–liquid interface.

For a given exposure time t (min), 430 mL of an RR120 solution was filled in the glass reactor at a distance of about 50 mm from the electrode tips. The solution was homogenized with magnetic stirrer. The selected input gas was moist air (gas flow rate optimized at 800 L h^{-1}).

The initial pH of the solution was 5.5 (RR120 solution pH). The solutions were exposed to the discharge for various times t = 0; 5; 10; 15; 30; 45; 60 min. After the exposure, an aliquot of the solution was immediately analyzed (UV–Vis and pH measurements). For the plasma-catalytic process, a desirable mass of TiO_2 was added to 50 mg L^{-1} dye solutions (430 mL). The mixture was then stirred for 30 min in the

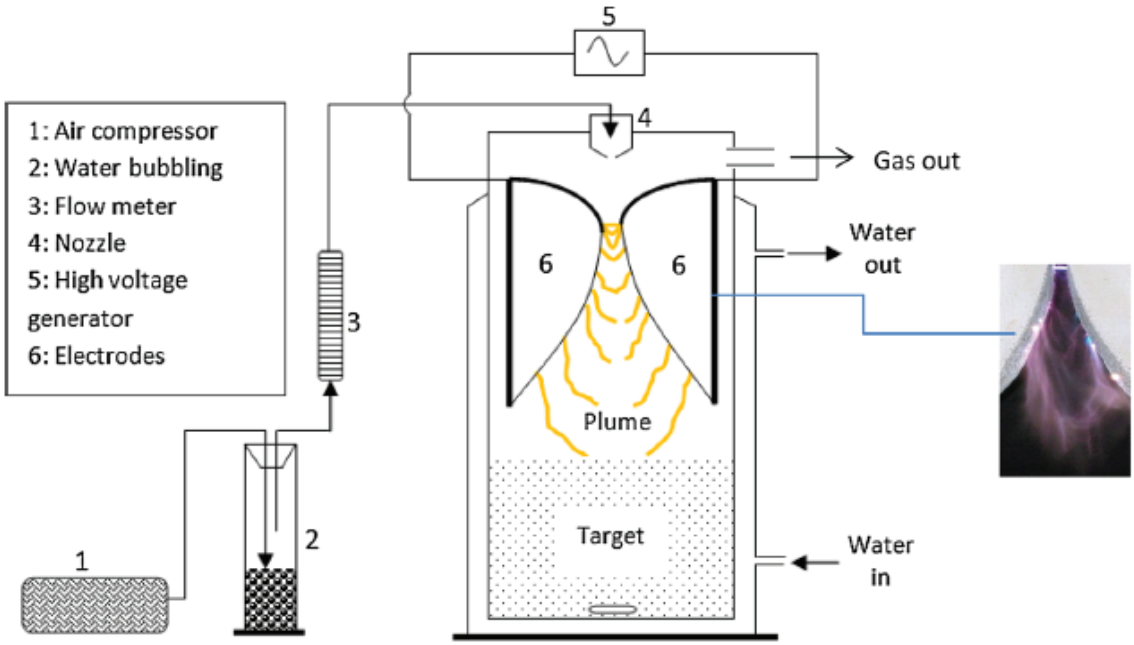

Fig. 1. Scheme of the gliding arc plasma reactor.

dark to complete the adsorption–desorption process before plasma treatment. After exposure to the plasma discharge for various times, the sample was centrifuged and analyzed. All the measurements were done in triplicate.

2.4. Analytical methods

Dye solution concentration was determined by measuring the solution absorbance at 534 nm using a "JENWAY" UV/VIS spectrometer recording the spectra. The discoloration efficiency was evaluated using the following formula:

$$\text{Discoloration efficiency (\%)} = \frac{C_0 - C}{C_0} \times 100 \quad (1)$$

where C_0 represents the initial concentration of the dye solution and C represents the concentration after each exposure time, t.

The pH measurement was performed on a portable HANNA HI 9811-5 electronic multi meter.

3. Results and discussion

3.1. Characterization of plasma-synthesized and Evonik P25 TiO_2

The TEM of plasma-synthesized and Evonik P25 TiO_2 are presented in Fig. 2. The images of Evonik P25 samples (Fig. 2(a)) reveal the typical spherical morphology of the particles and demonstrate that Evonik P25 TiO_2 crystals are nucleated from liquid phase (nano-droplets). In the case of plasma-synthesized TiO_2, the result shows that the morphology of the particles consists of anisotropic rods made of porous agglomerates.

The XRD diffractograms of the plasma-synthesized and commercial photocatalysts are depicted in Fig. 3. The crystallinity of these catalysts samples was clearly shown. The attribution of the peaks revealed that the material obtained is a mixture of anatase and rutile phase of TiO_2, which is interesting because it has been shown that a mixture of the two phases improves much more photocatalytic activity than each phase taken individually [39].

The commercial-P25 with specific surface of 50 m^2/g contains 70% anatase and 30% rutile and was purchased from Sigma-Aldrich (Belgium). Plasma synthesized TiO_2 consists of 21% anatase and 79% rutile. Its specific surface is 158 m^2/g [24]. The polymorphs composition is deduced from Spurr equation [40]:

$$f_R = 1 - \frac{1}{1 + 1{,}265\frac{I_R}{I_A}} \quad (2)$$

where f_R is the mass fraction of rutile, I_R and I_A are, respectively, the intensities of the main peaks of the rutile and anatase phase.

Fig. 4 shows the BET surface area of the plasma-synthesized TiO_2 calcined at 300°C; 400°C; 500°C; 600°C; 800°C and 1,000°C and the pore volume and pore size are gathered in Table 1. The commercial P25TiO_2 was used as reference.

The results reveal a decreasing trend with temperature. The surface area decreases up to 87% at 600°C, while the pore volume decrease of 47%. Heat treatment at 1,000°C during 3 h shows a surface area decrease of 97%, (5% corresponds to 4 m^2/g).

Table 1 summarizes the average pore diameter of the monometallic catalysts prepared. The highest increase in the pore width was observed for temperature up to 1,000°C. The anatase conversion into rutile is the reason of this pore opening.

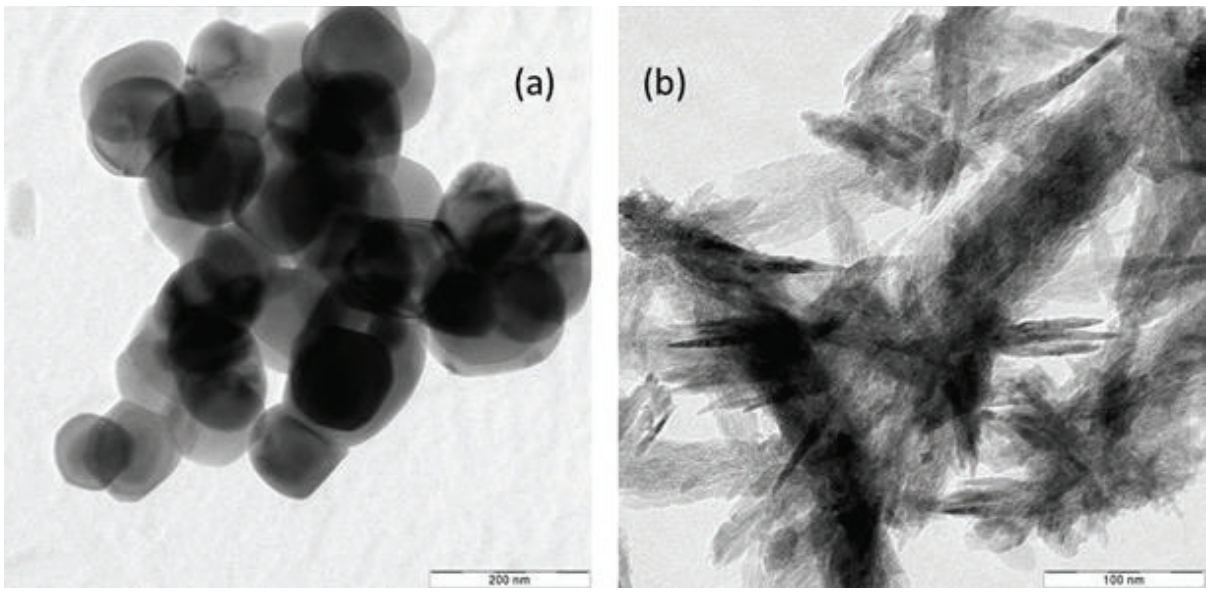

Fig. 2. TEM micrographs of Evonik P25 (a) and plasma-synthesized TiO_2 (b).

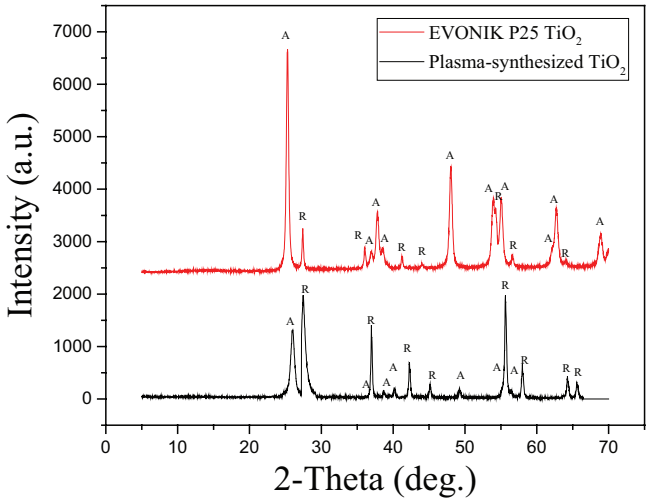

Fig. 3. Powder XRD patterns of P25 Evonik and plasma-synthesized TiO_2 (A: anatase, R: rutile).

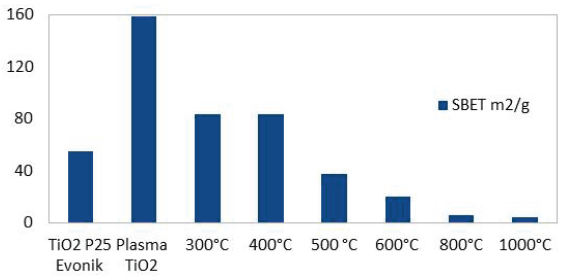

Fig. 4. Effect of calcination on the BET surface area of plasma-synthesized TiO_2.

The surface area and pore volume data obtained from the plasma synthesized TiO_2 samples calcined at various temperatures reveal that the sample can efficiently be used for catalytic applications only below 500°C.

Effect of calcination on the crystalline phase of plasma-synthesized TiO_2 samples

The XRD patterns obtained for the plasma-synthesized TiO_2 samples calcined at 300°C; 400°C; 500°C; 600°C; 800°C and 1,000°C (APMn, $n \geq 1$) and uncalcined plasma-synthesized TiO_2 (APM0) are shown in Fig. 5. We note a significant lowering of intensities for anatase peaks with temperature.

The increasing crystallite size can be quantified using the Scherrer equation: $B(2\theta) = \frac{k.\lambda}{L.\cos(\theta)}$ where the width of peak B is inversely proportional to the crystallite size L. The line (101) located at $2\theta = 35.7°$ is used because it is generally accepted that the best results are obtained using 2θ diffraction lines between 30° and 50°. The Scherrer constant of the diffractometer used is taken as 0.89. The visualization software and processing X-ray diffractometer, EVA directly provides the crystallite size values for each diffraction line chosen. Table 2 shows the characteristics of crystallite size of the plasma synthetized TiO_2 samples calcined at various temperatures.

In contrast to the effect of surface area and pore volume, the crystallite size shows an increasing trend with the calcination temperature.

A slight increase is observed up to 400°C, then a much larger increase with the calcination temperature above this temperature.

Hence, the heat treatment beyond 800°C showed a complete conversion of anatase into rutile and also a lowering of the surface area and pore volume; obviously the crystallite size increased.

3.2. Degradation of RR120 dye

The photocatalytic activity of nanorods synthesized by plasma was compared with commercial Evonik P25. All the experiments involving the catalyst were initially agitated in the dark during 30 min for the dye to attain adsorption–desorption equilibrium and to ensure reproducibility of the results. In order to compare the performance of different photocatalysts, experiments of photo-degradation are

Table 1
BET surface area, pore volume and pore size of plasma-synthesized TiO_2 (APMn, $n \geq 0$) and commercial P25 Evonik samples

Samples	Calcination temperature	Calcination time	BET surface area (m^2/g)	Pore volume (cm^3/g)	Pore size (nm)
TiO_2 P25	Uncalcined	–	54.65	0.274	19.20
Plasma TiO_2	Uncalcined	–	158.27	0.247	8.67
APM1	300°C	3 h	83.33	0.226	9.31
APM2	400°C	3 h	83.73	0.266	10.70
APM3	500°C	3 h	37.14	0.168	15.58
APM4	600°C	3 h	20.44	0.137	24.59
APM5	800°C	3 h	5.50	0.034	33.25
APM6	1,000°C	3 h	4.00	0.016	33.95

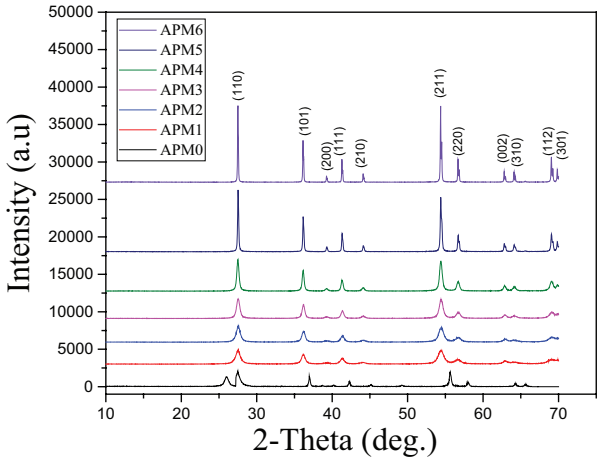

Fig. 5. Powder XRD patterns of uncalcinated (APM0) and calcined plasma-synthesized TiO_2 (APMn, $n \geq 1$).

Table 2
Crystallite size of plasma-synthesized TiO_2 (APMn, $n \geq 0$) samples

Samples	Calcination temperature	Calcination time	Crystallite size (Å)
APM0	Uncalcined	–	132
APM1	300°C	3 h	137
APM2	400°C	3 h	148
APM3	500°C	3 h	199
APM4	600°C	3 h	288
APM5	800°C	3 h	499
APM6	1,000°C	3 h	620

carried out in the same reactor with an initial concentration of to 50 mg/L.

3.2.1. Determination of the catalyst optimal mass

The catalyst concentration was varied from 0.1 to 2 g L^{-1}, the results (Fig. 6) show that degradation, increased with treatment time and the resulting adequate catalyst amount is 1 g L^{-1}. Only a slight enhancement was observed when TiO_2 concentration further increased to 2 g L^{-1}. However, it was observed that above a certain level of concentration, the reaction rate decreases and becomes independent of the catalyst concentration. This observation can be attributed to the availability of active sites on TiO_2 surface and to the light penetration into the suspension. For the concentration lower than 1 g L^{-1}, the observed enhancement in discoloration is probably due to an increased number of available adsorption and catalytic sites on TiO_2. The availability of active sites increases with the suspension of catalyst loading, but the light penetration, and hence, the photoactivated volume of the suspension shrinks. A further increase in catalyst loading, however, may cause light scattering and screening effect and thus reducing the specific activity of the catalyst. Moreover, the decrease in the percentage of degradation at higher catalyst loading may be due to deactivation of activated molecules by collision with ground state molecules. In addition, agglomeration and sedimentation of the TiO_2 particles could also occur and part of the catalyst surface probably becomes unavailable for photon absorption and dye adsorption, thus bringing little stimulation to the catalytic reaction.

3.2.2. Comparison of plasma-synthesized and P25 TiO_2

The addition of TiO_2 (1 g L^{-1}) catalyst improves the discoloration rate up to 35% with the commercial P25 and to 98% for the TiO_2-synthesized by plasma as shown in Fig. 7. The blank test (without a catalyst) gives 24% after 60 min. The degradation rate in this case depends on the in-situ generated oxidizing species such as $HO^{\bullet}$ = 2.85 V/SHE formed in the plasma arc. Moreover, the degradation of RR120 is much faster in the presence of TiO_2 prepared by plasma than that of TiO_2 P25 (Fig. 7).

In order to monitor the disappearance of the RR120 absorption band and the eventual appearance of new absorption bands, absorption spectra were recorded in the UV-Vis domain during the reaction. As results, whatever the catalyst used as can be seen in Figs. 8(a) and (b), respectively, for TiO_2 P25 and plasma-synthesized TiO_2, there is a gradual and simultaneous decrease in the intensity of the absorption band at 525 nm. The results came to corroborate the previous ones. It does not appear of new absorption band indicating that the degradation begins by breaking the conjugation of this molecule (original red color) and there is no middleman stable retaining structure (with side chain degradation). One might assume as an intermediate species having one or two aromatic rings which are not detected because they appear below 300 nm.

This study gives to understand that the combination of plasma Glidarc technique and photocatalysis can be

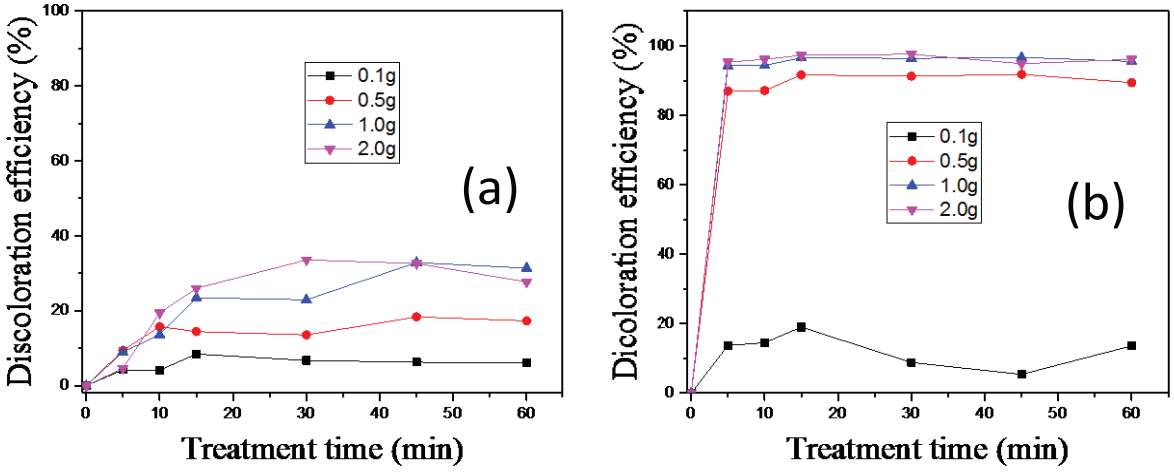

Fig. 6. Effect of P25 (a) and plasma-synthesized (b) TiO_2 catalyst amount on the discoloration efficiency.

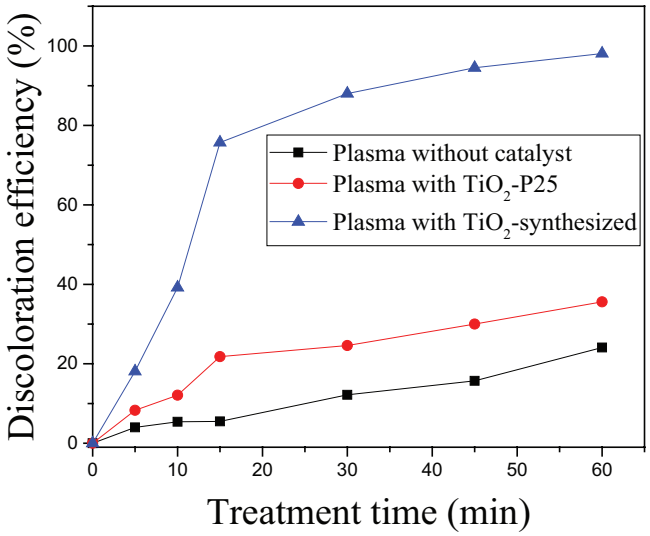

Fig. 7. Comparison of discoloration of RR120 dye without and with TiO_2 catalysts (1.0 g L^{-1}).

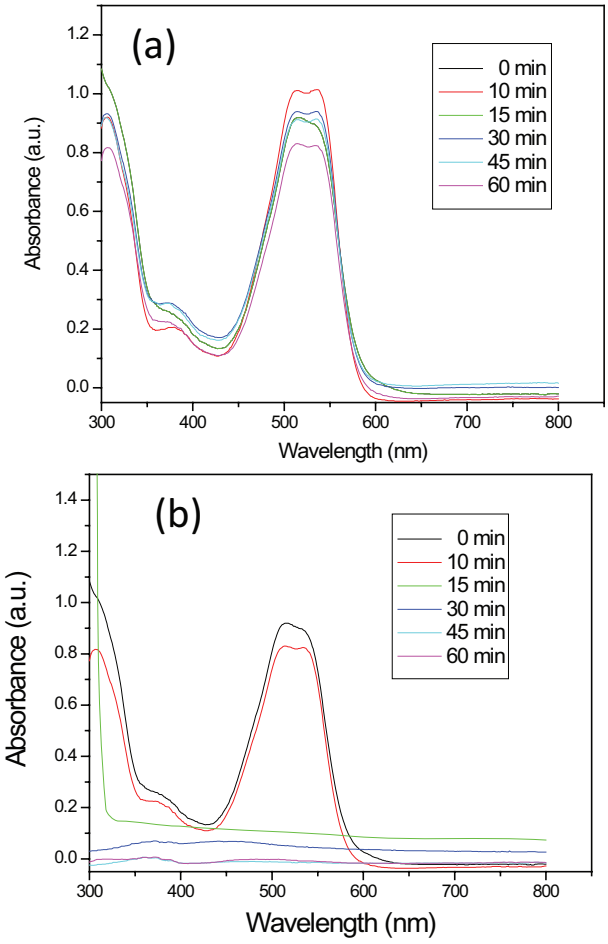

Fig. 8. UV–Vis spectra of RR120 dye treated with (a) TiO_2 P25 catalyst and (b) plasma synthetized TiO_2 catalyst.

used in order to improve the degradation of RR120 dye. As can be seen from UV–Vis diffuse spectra in Fig. 9, the photocatalytic activity of plasma synthesized TiO_2, being significantly higher is due to the fact that compared with the commercial P25, which is active only under UVB light (280–320 nm), the plasma synthesized TiO_2 exhibit an enhanced activity under UVA (λ = 320–400 nm). This is very interesting because the measurement of the UV radiation flux emitted in the glidarc reactor has shown no emission in the interval of 200–300 nm but important ultraviolet peaks are recorded at 364.5, 388.5, 388.9, and 397 nm wavelengths [41,42].

Concerning the influence of temperature of calcination on the photocatalytic activity, the synthesized TiO_2 was calcined between 300°C and 1,000°C. The discoloration efficiency for both photocatalysts (after 15 min of reaction) vs. the calcination temperature is shown in Fig. 10.

Whatever the sample, the increase of temperature negatively affects the photocatalytic efficiency, thus corroborating previously observed rutilation with temperature increase knowing that taken alone the anatase form is 10-fold more efficient than rutile. Besides, it is clear from this figure that the plasma synthesized sample presents an important drop in efficiency around 500°C, with almost 70% in contrary of

P25 which presents a gradual decreasing trend. The plasma synthesized sample seems then less stable due probably to the lower amount of anatase phase.

4. Stability and reusability

From Fig. 11 it appears that after three cycles, TiO_2-synthesized recycles less than the commercial P25 with 25% and 2% loss in efficiency, respectively. This discrepancy probably comes from the difference in size between both samples, given that the TiO_2-synthesized by plasma with nanoscale size is more difficult to recover. This drawback is a crucial problem because it is often expensive to separate TiO_2 nanomaterials from treated wastewater and the nanoparticles are generally found in the environment or in biological systems. Thus, to overcome these problems, the developments of new heterojunctions either by incorporating secondary semiconductor metal or carbon quantum dot nanoparticles are some major strategies to be implemented [43,44]. However, it is to be noted that the TiO_2 keeps all its physical integrity as evidenced by the SEM images. The morphology of TiO_2 particles after the plasmachemical catalytic test remains identical to that of the fresh photocatalysts shown in the following SEM for commercial-P25 and plasma synthesized TiO_2. Moreover, its effectiveness remains significant because despite this mass loss we reach a yield of 75% after three cycles.

5. Conclusions

The non-thermal plasma generated by gliding arc discharge is successfully applied to synthesize TiO_2 nanopowders. The morphology of plasma synthesized TiO_2 particles consists of anisotropic rods of porous agglomerates and shows that these rods have a length of 50–100 nm and a

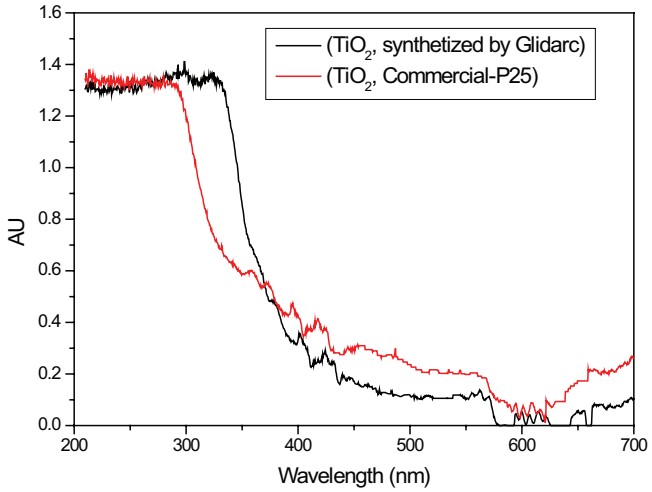

Fig. 9. UV–Vis diffuse reflectance spectra of commercial-P25 and plasma-synthesized TiO_2.

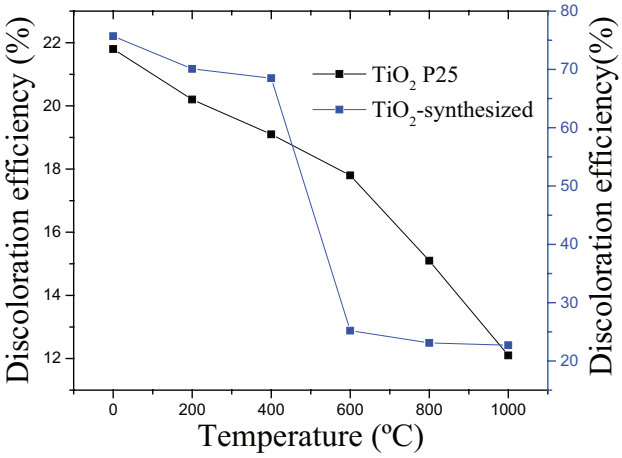

Fig. 10. Influence of calcination on the discoloration rate of RR120 dye.

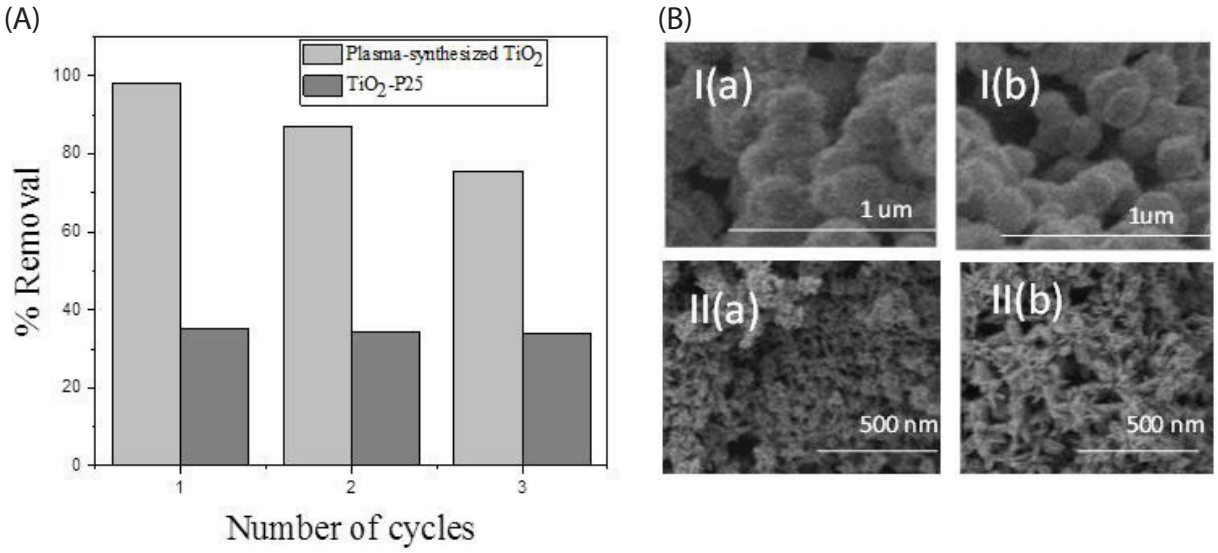

Fig. 11. Discoloration efficiency after three cycles (A) and SEM micrographs (B) of Evonik P25 (I) and plasma-synthesized TiO_2 (II) before (a) and after use (b).

diameter of 5–15 nm. The effect of calcination has been studied by XRD, nitrogen adsorption–desorption isotherm, BET-surface area, pore volume, pore size and crystallite size. The effect of rutilation is significant as the temperature increase. At 1,000°C, the diameter of the nanoparticles is approximately 34 nm with a specific surface area of 4 m^2/g. The pore volume shows a large decrease at 1,000°C up to 93.5% during 3 h of heat treatment. The initial polluted solution with 50 mg L^{-1} of RR120 is discolored up to 24% after 60 min of in situ treatment and without a catalyst. The degradation rate in this case depends on generating highly oxidizing species; the addition of TiO_2 catalyst improves the discoloration rate up to 35% with the commercial and 98% for the TiO_2-synthesized by plasma. This comparative study suggests that the photo-catalyst TiO_2 nanorods synthesized by plasma are actually technically more efficient than commercial TiO_2 to improve pollutant abatement.

Acknowledgments

The authors would like to express their gratitude to the International Foundation of Science (IFS) for the Jenway spectrophotometer granted to S.N.

References

[1] C.R. Holkar, A.J. Jadhav, D.V. Pinjari, N.M. Mahamuni, A.B. Pandit, A critical review on textile wastewater treatments: possible approaches, J. Environ. Manage., 182 (2016) 351–366.
[2] D. Brown, P. Laboureur, The degradation of dyestuffs: Part I. Primary biodegradation under anaerobic conditions, Chemosphere 12 (1983) 397–404.
[3] E. Forgacs, T. Cserhati, G. Oros, Removal of synthetic dyes from wastewaters: a review, Environ. Int., 30 (2004) 953–971.
[4] V.K. Gupta, R. Saravanan, S. Agarwal, F. Gracia, M.M. Khan, J. Qin, R.V. Mangalaraja, Degradation of azo dyes under different wavelengths of UV light with chitosan-SnO_2 nanocomposites, J. Mol. Liq., 232 (2017) 423–430.
[5] M. Thakur, G. Sharma, T. Ahamad, A.A. Ghfar, D. Pathania, M. Naushad, Efficient photocatalytic degradation of toxic dyes from aqueous environment using gelatin-Zr(IV) phosphate nanocomposite and its antimicrobial activity, Colloids Surf., B, 157 (2017) 456–463.
[6] A.A. Alqadami, M. Naushad, Z.A. Alothman, T. Ahamad, Adsorptive performance of MOF nanocomposite for methylene blue and malachite green dyes: kinetics, isotherm and mechanism, J. Environ. Manage., 223 (2018) 29–36.
[7] E. Daneshvar, A. Vazirzadeh, A. Niazi, M. Kousha, M. Naushad, A. Bhatnagar, Desorption of Methylene blue dye from brown macroalga: effects of operating parameters, isotherm study and kinetic modeling, J. Cleaner Prod., 152 (2017) 443–453.
[8] A.C. Sophia, E.C. Lima, Removal of emerging contaminants from the environment by adsorption, Ecotoxicol. Environ. Saf., 15 (2018) 1–17.
[9] D. Tadom, G. Kamgang-Youbi, E. Acayanka, E. Njoyim-Tamungang, S. Laminsi, Reduction of sludge formed during a coagulation treatment of Ridomil Gold by means of non-thermal quenched plasma pre-treatment, Environ. Monit. Assess., 190 (2018) 443.
[10] J.B. Tarkwa, N. Oturan, E. Acayanka, S. Laminsi, M.A. Oturan, Photo-Fenton oxidation of Orange G azo dye: process optimization and mineralization mechanism, Environ. Chem. Lett., (2018) 1–7. DOI:10.1007/s10311-018-0773-0.
[11] J.-M. Herrmann, Heterogeneous photocatalysis: fundamentals and applications to the removal of various types of aqueous pollutants, Catal. Today, 53 (1999) 115–129.
[12] M.I. Litter, Heterogeneous photocatalysis transition metal ions in photocatalytic systems, Appl. Catal., B, 23 (1999) 89–114.
[13] A. Fujishima, T.N. Rao, D.A. Tryk, Titanium dioxide photocatalysis, J. Photochem. Photobiol. C, 1 (2000) 1–21.
[14] D.S. Bhatkhande, V.G. Pangarkar, A.ACM. Beenackers, Photocatalytic degradation for environmental applications – a review, J. Chem. Technol. Biotechnol., 77 (2002) 102–116.
[15] Y. Boyjoo, H. Sun, J. Liu, V.K. Pareek, S. Wang, A review on photocatalysis for air treatment: from catalyst development to reactor design, Chem. Eng. J., 310 (2017) 537–559.
[16] X. Chen, S. Samuel Mao, Titanium dioxide nanomaterials: synthesis, properties, modifications, and application, Chem. Rev., 7 (2007) 2891–2959.
[17] K. Nakata, A. Fujishima, TiO_2 photocatalysis: design and applications, J. Photochem. Photobiol. C, 13 (2012) 169–189.
[18] J.K. Jiang, D.R. Chen, P. Biswas, Synthesis of nanoparticles in a flame aerosol reactor with independent and strict control of their size, crystal phase and morphology, Nanotechnology, 18 (2007) 285603.
[19] J. Schneider, M. Matsuoka, M. Takeuchi, J. Zhang, Y. Horiuchi, M. Anpo, D.W. Bahnemann, Understanding TiO_2 photocatalysis: mechanisms and materials, Chem. Rev., 114 (2014) 9919–9986.
[20] M.R. Hoffmann, S.T. Martin, W. Choi, D.W. Bahnemann, Environmental applications of semiconductor photocatalysis, Chem. Rev., 95 (1995) 69–96.
[21] A. Tiya-Djowe, N. Ruth, G. Kamgang-Youbi, E. Acayanka, S. Laminsi, E.M. Gaigneaux, FeO x -kaolinite catalysts prepared via a plasma-assisted hydrolytic precipitation approach for Fenton-like reaction, Microporous Mesoporous Mater., 255 (2017) 148–155.
[22] F.W. Boyom-Tatchemo, S. Nzali, G. Kamgang-Youbi, A. Tiya-Djowe, D. Kuete-Saa, E. Acayanka, S. Laminsi, E.M. Gaigneaux, Gliding arc plasma synthesis of MnO_2 nanorods for the plasma-catalytic bleaching of azoic amaranth red dye, Topics Catal., 60 (2017) 962–972.
[23] V. Smeets, L.B. Mustapha, J. Schnee, E.M. Gaigneaux, D.P. Debecker, Mesoporous SiO_2-TiO_2 epoxidation catalysts: tuning surface polarity to improve performance in the presence of water, Mol. Catal., 452 (2018) 123–128.
[24] E. Acayanka, A. Tiya Djowe, S. Laminsi, C.C. Tchoumkwé, S. Nzali, P.A. Mbouopda, P.T. Ndifon, E.M. Gaigneaux, Plasma-assisted synthesis of TiO_2 nanorods by gliding arc discharge processing at atmospheric pressure for photocatalytic applications, Plasma Chem. Plasma Process., 33 (2013) 725–735.
[25] H. Lesueur, A. Czernichowski, J. Chapelle, Dispositif de génération de plasma basse, température par formation de décharges électriques glissantes, French patent 2,639,17, 1988.
[26] A. Czernichowski, GlidArc Assisted preparation of the synthesis gas from natural and waste hydrocarbons gases, Oil & Gas Sci. Technol. – Rev. IFP, 56 (2001) 181–198.
[27] L. Delair, J.-L. Brisset, B.J. Cheron, Spectral electrical and dynamical analysis of a 50 Hz air gliding arc, High Temp. Mater. Process., 20 (2001) 381–402.
[28] J. Fanmoe, J.O. Kamgang, D. Moussa, J.-L. Brisset, Application de l'arc glissant d'air humide au traitement des solvants industriels: cas du 1, 1, 1-trichloroethane, Phys. Chem. News, 14 (2003) 1–4.
[29] A. Doubla, S. Laminsi, S. Nzali, E. Njoyim, J. Kamsu-Kom, J.L. Brisset, Organic pollutant abatement and bio-decontamination of brewery effluents by non-thermal plasma at atmospheric pressure, Chemosphere, 69 (2007) 332–337.
[30] J.L. Brisset, D. Moussa, A. Doubla, E. Hnatiuc, B. Hnatiuc, G. Kamgang-Youbi, J.M. Herry, M. Naitali, M.N. Bellon-Fontaine, Chemical reactivity of discharges and temporal post-discharges in plasma treatment of aqueous media: examples of gliding arc discharge treated solutions, Ind. Eng. Chem. Res., 47 (2008) 5761–5781.
[31] M.R. Ghezzar, F. Abdelmalek, M. Belhadj, N. Benderdouche, A. Addou, Enhancement of the bleaching and degradation of textile wastewaters by Gliding arc discharge plasma in the presence of TiO_2 catalyst, J. Hazard. Mater., 164 (2009) 1266–1274.
[32] D.A. Tiya, E. Acayanka, N.R.G. Lontio, S. Laminsi, E.M. Gaigneaux, Enhanced discolouration of Methyl Violet 10B in a gliding arc plasma reactor by the maghemite nanoparticles

used as heterogeneous catalyst, J. Environ. Chem. Eng., 3 (2015) 953–960.
[33] D. Moussa, A. Doubla, G. Kamgang-Youbi, J.L. Brisset, Post-discharge long life reactive intermediates involve in the plasma-chemical degradation of an azoic dye, IEEE Trans. Plasma Sci., 35 (2007) 444–453.
[34] L.D.T. Prola, E. Acayanka, E.C. Lima, C. BestettiWmekson Oliveira Santos, F.A. Pavan, S.L.P. Dias, C.R.T. Tarley, Application of aqai stalks as biosorbent for the removal of Evans Blue and Vilmafix Red RR-2B dyes from aqueous solutions, Desal. Wat. Treat., 51 (2013) 1–11.
[35] B.H. Mansour, D. Corroler, D. Barillier, K. Ghedira, L. Chekir, R. Mosrati, Evaluation of genotoxicity and pro-oxidant effect of the azo dyes: acids yellow 17, violet 7 and orange 52, and of their degradation products by *Pseudomonas putida* mt-2, Food Chem. Toxicol., 45 (2007) 1670–1677.
[36] J.L. Brisset, J. Pawlat, Chemical effects of air plasma species on aqueous solutes in direct and delayed exposure modes: discharge, post-discharge and plasma activated water, Plasma Chem. Plasma Process., 36 (2016) 355–381.
[37] B. Benstaali, P. Boubert, B.G. Cheron, A. Addou, J.L. Brisset, Density and rotational temperature measurements of the OH^{o} and NO^{o} radicals produced by a gliding arc in humid air, Plasma Chem. Plasma Process., 22 (2002) 553–571
[38] S. Laminsi, E. Acayanka, S. Nzali, P.T. Ndifon, J.L. Brisset, Direct impact and delayed post-discharge chemical reactions of FeII complexes induced by non-thermal plasma, Desal. Wat. Treat., 37 (2012) 38–45.
[39] J. Yu, X. Zhao, Q. Zhao, Effect of surfaces structures on photocatalytic activity of TiO_2 thin films prepared by sol-gel method, Thin Solid Films, 379 (2000) 7–14.
[40] R.A. Spurr, H. Myers, Quantitative analysis of anatase-rutile mixtures with an X-ray diffractometer, Anal. Chem., 29 (1957) 760–762.
[41] M. Gharagozalian, D. Dorranian, M. Ghoranneviss, Water treatment by the AC gliding arc air plasma, J. Theor. Appl. Phys., 11 (2017) 171–180.
[42] P.J. Bruggeman, M.J. Kushner, B.R. Locke, J.G.E. Gardeniers, W.G. Graham, D.B. Graves, R.C.H.M. Hofman-Caris, D. Maric, J.P. Reid, E. Ceriani, D. Fernandez Rivas, J.E. Foster, S.C. Garrick, Y. Gorbanev, S. Hamaguchi, F. Iza, H. Jablonowski, E. Klimova, J. Kolb, F. Krcma, P. Lukes, Z. Machala, I. Marinov, D. Mariotti, S. Mededovic Thagard, D. Minakata, E.C. Neyts, J. Pawlat, Z. Lj Petrovic, R. Pflieger, S. Reuter, D.C. Schram, S. Schröter, M. Shiraiwa, B. Tarabová, P.A. Tsai, J.R.R. Verlet, T. von Woedtke, K.R. Wilson, K. Yasui, G. Zvereva Plasma–liquid interactions: a review and roadmap, Plasma Sources Sci. Technol., 25 (2016) 053002.
[43] E. Acayanka, D.S. Kuete, G.Y. Kamgang, S. Nzali, S. Laminsi, P.T. Ndifon, Synthesis, characterization and photocatalytic application of TiO_2/SnO_2 nanocomposite obtained under non-thermal plasma condition at atmospheric pressure, Plasma Chem. Plasma Process., 36 (2016) 799–811.
[44] A. Kumar, A. Kumar, G. Sharma, A.H. Al-Muhtaseb, M. Naushad, A.A. Ghfar, C. Guo, F.J. Stadler, Biochar-templated $g\text{-}C_3N_4/Bi_2O_2CO_3/CoFe_2O_4$ nano-assembly for visible and solar assisted photo-degradation of paraquat, nitrophenol reduction and CO_2 conversion, Chem. Eng. J., 339 (2018) 393–410.